# Supplementary Information

## Geometry Scaling of Thermal Boundary Resistance in Plasmonic Nanostructures

Zoe Bradley[1], Abhijit Ganguly[1], Bas Heitzer[2], Jaap Drenth[2], and Nikhil Bhalla*[1]

[1]Nanotechnology and Integrated Bioengineering Centre (NIBEC), School of Engineering, Ulster University, 2-24 York Street, Belfast BT15 1AP, Northern Ireland, United Kingdom
[2]Sensip-dx, Oxfordlaan 70, 6229 EV Maastricht, Netherlands

*Corresponding author: n.bhalla@ulster.ac.uk

# Contents

# 1 Geometry Scaling of Thermal Boundary Resistance in Plasmonic Nanostructures

In the following derivation, the heat capacities are expressed per unit volume. Accordingly, the absorbed optical power and heater power are treated as volumetric power densities, $P_{\mathrm{abs}}(t)$ and $P_0$, with units of $\mathrm{W,m^{-3}}$. Consequently, the resistance obtained from the relaxation time is the volume-normalised resistance, $R_{\mathrm{th,vol}}$. To model the heat-transfer resistance, we first define the electron subsystem of the nanoparticles by Eq. S1:

$$C_e \frac{dT_e}{dt} = -G(T_e - T_\ell) + P_{\mathrm{abs}}(t) \tag{S1}$$

Here, $G$ is the volumetric electron–phonon coupling coefficient, and $P_{\mathrm{abs}}(t)$ is the volumetric power-density component from light absorption, which is zero in the dark and nonzero under LSPR illumination. $T_\ell$, $T_e$, and $C_e$ are the lattice temperature, electron temperature, and electronic heat capacity of the system, respectively. In this reduced model, $C_e$ is treated as constant over the small temperature range of the experiment. The minus sign in the $-G(T_e - T_\ell)$ term of Eq. S1 reflects that this coupling is a loss of energy for the electron subsystem. Defining the inter-subsystem volumetric heat-transfer rate density from electrons to lattice as $J_{e\to\ell} \equiv G(T_e - T_\ell)$, which is positive when $T_e > T_\ell$, Eq. S1 contains $-J_{e\to\ell}$.. .

The lattice subsystem, through which heat is transferred to the surrounding fluid, is defined by Eq. S2:

$$C_\ell \frac{dT_\ell}{dt} = G(T_e - T_\ell) - \frac{T_\ell - T_b}{R_{\mathrm{th,vol}}} \tag{S2}$$

In Eq. S2, the same coupling appears with a plus sign, $+G(T_e - T_\ell) = +J_{e\to\ell}$, because it is a gain of energy for the lattice. With this sign convention, adding Eqs. S1 and S2 cancels the $\pm G(T_e - T_\ell)$ terms and yields conservation of total internal energy:

$$C_e \frac{dT_e}{dt} + C_\ell \frac{dT_\ell}{dt} = P_{\mathrm{abs}}(t) - \frac{T_\ell - T_b}{R_{\mathrm{th,vol}}} \tag{S3}$$

This sign convention also guarantees linear stability of the electron–lattice temperature difference, i.e., $T_e - T_\ell \to 0$ for $G > 0$.

It should be noted that the electronic heat-capacity term is not neglected in the full two-temperature energy balance. When Eqs. S1 and S2 are added, the electron–phonon coupling terms cancel because they describe internal energy exchange between the electron and lattice subsystems, while the energy-storage terms remain. The later reduction to a single-temperature model follows from the strong electron–phonon coupling limit, where electron–lattice equilibration is much faster than the experimentally measured thermal relaxation.

$C_\ell$ is the lattice heat capacity, and $T_b = 37°\mathrm{C}$ is fixed by heater power $P_0$ in the microfluidic system.

To calculate $C_\ell$, the density of gold is taken as

$$\rho_{\mathrm{Au}} = 19.32 \times 10^3\,\mathrm{kg\,m^{-3}}. \tag{S4}$$

The specific heat capacity of gold at room temperature is

$$c_{p,\mathrm{Au}} \approx 129\,\mathrm{J\,kg^{-1}\,K^{-1}}. \tag{S5}$$

The volumetric lattice heat capacity is therefore given by

$$C_\ell = \rho_{\mathrm{Au}} \times c_{p,\mathrm{Au}}. \tag{S6}$$

Thus,

$$C_\ell = \left(19.32 \times 10^3\,\mathrm{kg\,m^{-3}}\right)\left(129\,\mathrm{J\,kg^{-1}\,K^{-1}}\right) = 2.49 \times 10^6\,\mathrm{J\,m^{-3}\,K^{-1}}. \tag{S7}$$

Please note that $C_\ell$ calculated in Eq. S7 is the volumetric lattice heat capacity.

We now define the measured thermal resistance as the sum of the nanoparticle–fluid interfacial resistance, $R_{\mathrm{int}}$, and the device-level fluid resistance, $R_{\mathrm{fluid}}$:

$$R_{\mathrm{th}} = R_{\mathrm{int}} + R_{\mathrm{fluid}}. \tag{S8}$$

Because the heat capacity used above is volumetric, the resistance extracted from the relaxation time is written in volume-normalised form as

$$R_{\mathrm{th,vol}} = R_{\mathrm{int,vol}} + R_{\mathrm{fluid,vol}}. \tag{S9}$$

Here, $R_{\mathrm{th,vol}}$ represents the total thermal resistance normalised by the probed fluid volume. It contains both the nanoparticle–liquid interfacial contribution, $R_{\mathrm{int,vol}}$, and the device-level fluid contribution, $R_{\mathrm{fluid,vol}}$. Thus, $R_{\mathrm{th,vol}}$ is the experimentally extracted volumetric resistance of the nanoparticle suspension, whereas $R_{\mathrm{int,vol}}$ is obtained after subtracting the independently measured buffer/fluid baseline.

The interfacial volumetric contribution is defined as

$$R_{\mathrm{int,vol}} = N_p\,\frac{V_{\mathrm{NP}}}{A_{\mathrm{NP}}}\,R_{K0}\left(\frac{D}{L} + \alpha\,\frac{h_{\mathrm{spike}}}{r_{\mathrm{tip}}}\right). \tag{S10}$$

In Eq. S10, $N_p$ is the total number of nanoparticles within the probed fluid volume, $V_{\mathrm{NP}}$ is the volume of an individual nanoparticle, and $A_{\mathrm{NP}}$ is the surface area of an individual nanoparticle. The ratio $V_{\mathrm{NP}}/A_{\mathrm{NP}}$ represents a characteristic geometric length scale and encodes the base size dependence of the particle before the shape correction is applied. The bracketed term, $(D/L + \alpha h_{\mathrm{spike}}/r_{\mathrm{tip}})$, represents the dimensionless morphology factor. For nanospheres, $D = L$ and the spike term is zero, so the morphology factor reduces to unity. For nanorods, the factor is governed by the aspect ratio $D/L$, whereas for nanostars it includes the additional curvature contribution from the spike height $h_{\mathrm{spike}}$ and tip radius $r_{\mathrm{tip}}$.

Here, $R_{K0}$ denotes the baseline Kapitza resistance per unit area for the Au–buffer interface. It is treated as a material/interfacial reference parameter that is independent of nanoparticle geometry in the present model. The buffer-only measurement is used to determine the device/fluid contribution, $R_{\mathrm{fluid,vol}}$, and does not directly measure $R_{K0}$ because no Au–buffer nanoparticle interface is present in the buffer-only control. In the present analysis, we use

$$R_{K0} = 5 \times 10^{-9}\,\mathrm{m^2K/W}.$$

This value is obtained by taking the reciprocal of a representative Au–water/Au–buffer interfacial thermal conductance,

$$G_{K0} = 200\,\mathrm{MW\,m^{-2}K^{-1}} = 2 \times 10^{8}\,\mathrm{W\,m^{-2}K^{-1}},$$

such that

$$R_{K0} = \frac{1}{G_{K0}} = \frac{1}{2 \times 10^{8}} = 5 \times 10^{-9}\,\mathrm{m^{2}K/W}.$$

This value lies within the order of magnitude reported for Au–water and gold-nanoparticle–water interfaces. Previous molecular dynamics and nanoscale heat-transfer studies have shown that interfacial thermal conductance at nanoparticle–water and metal–water interfaces is typically in the range of $10^{1}$–$10^{2}\,\mathrm{MW\,m^{-2}K^{-1}}$ to a few $10^{2}\,\mathrm{MW\,m^{-2}K^{-1}}$, depending on nanoparticle size, wetting state, ligand/surface chemistry, surface charge, and the structure of interfacial water [1, 2, 3, 4]. Therefore, $R_{K0} = 5 \times 10^{-9}\,\mathrm{m^{2}K/W}$ is used here as a literature-consistent Au–buffer reference value rather than as a morphology-specific fitting parameter.

We treat $R_{K0}$ as identical across nanospheres, nanorods, and nanostars because the particle material, buffer, measurement cell, temperature range, and thermal protocol were kept fixed. This assumption allows the shape-dependent part of the response to be isolated through the geometry factor. If required, the scaling relation can also be inverted to obtain apparent morphology-specific values, $R_{K0}^{\mathrm{eff}}$, but these are treated as diagnostic interfacial parameters rather than as inputs used to force the master scaling collapse. For different metals, ligand shells, surface charges, solvents, ionic strengths, or strongly modified interfacial chemistries, $R_{K0}$ should be independently re-determined (using literature or experiment) or sensitivity-tested.

The fluid volumetric contribution is

$$R_{\mathrm{fluid,vol}} = \frac{V_{\mathrm{fluid}}}{h_{\mathrm{conv}}\,A_{\mathrm{cell}}} \tag{S11}$$

Using Eqs. S9–S11 gives

$$R_{\mathrm{th,vol}} = N_p\,\frac{V_{\mathrm{NP}}}{A_{\mathrm{NP}}}\,R_{K0}\left(\frac{D}{L} + \alpha\,\frac{h_{\mathrm{spike}}}{r_{\mathrm{tip}}}\right) + \frac{V_{\mathrm{fluid}}}{h_{\mathrm{conv}}\,A_{\mathrm{cell}}}. \tag{S12}$$

Table S1 summarises the symbols and their units.

The heat resistance of the fluid, $R_{\mathrm{fluid}}$ (i.e., the buffer), is measured from the experiment as $R_{\mathrm{fluid}} = 5.5$ K/W. Using this and Eq. S11, we determine the convective heat-transfer coefficient, $h_{\mathrm{conv}}$, of the fluid and the corresponding volumetric fluid resistance. To convert the measured fluid resistance to a volume-normalised resistance, we multiply by the fluid volume:

$$R_{\mathrm{fluid,vol}} = R_{\mathrm{fluid}} \times V_{\mathrm{fluid}} = 5.5\,\mathrm{K\,W^{-1}} \times 2.00 \times 10^{-7}\,\mathrm{m^{3}} = 1.10 \times 10^{-6}\,\mathrm{m^{3}\,K\,W^{-1}}. \tag{S13}$$

It is important to note that $R_{\mathrm{fluid,vol}}$ is an independently measured device/buffer baseline obtained from the control measurement in the same measurement cell, rather than a morphology-dependent fitting parameter. Therefore, its subtraction removes a common additive contribution from all nanoparticle measurements. A fixed offset of this type cannot by

| Symbol | Description | Unit |
|---|---|---|
| $R_{\mathrm{th,vol}}$ | Total volume-normalised thermal resistance | K·m$^3$/W |
| $R_{\mathrm{int,vol}}$ | Volume-normalised nanoparticle–fluid interfacial resistance | K·m$^3$/W |
| $R_{\mathrm{fluid,vol}}$ | Volume-normalised fluid/device resistance | K·m$^3$/W |
| $N_p$ | Total number of nanoparticles within the probed fluid volume | – |
| $A_{\mathrm{NP}}$ | Surface area of an individual nanoparticle | m$^2$ |
| $V_{\mathrm{NP}}$ | Volume of an individual nanoparticle | m$^3$ |
| $R_{K0}$ | Baseline Kapitza resistance per unit area for the Au–buffer interface | K·m$^2$/W |
| $\alpha$ | Geometrical correction factor | – |
| $r_{\mathrm{tip}}$ | Tip radius of nanoparticle spikes | m |
| $h_{\mathrm{spike}}$ | Height of nanoparticle spikes | m |
| $V_{\mathrm{fluid}}$ | Volume of surrounding fluid | m$^3$ |
| $h_{\mathrm{conv}}$ | Convective heat-transfer coefficient | W/(m$^2$K) |
| $A_{\mathrm{cell}}$ | Surface area of the fluid cell | m$^2$ |
| $D$ | Nanoparticle diameter, rod diameter, or star-core diameter | m |
| $L$ | Nanoparticle length; for spheres $L = D$, for rods $L$ is the rod length, and for stars $L = D_{\mathrm{core}} + 2h_{\mathrm{spike}}$ | m |

Table S1: Description of parameters in the volumetric thermal resistance model, Eq. S12.

itself generate the observed morphology-dependent ordering, because the relative differences between nanospheres, nanorods, and nanostars are already present in the measured total resistance before subtraction. The subtraction instead isolates the nanoparticle-associated contribution from the common macroscopic fluid pathway of the device.

Although local illumination may in principle modify near-particle viscosity, buoyancy, or microscale thermal transport, the measurement volume, cell geometry, temperature boundary condition, and illumination protocol were kept identical for all morphologies, and dark and illuminated datasets were analysed separately. Thus, any residual fluid contribution associated with a given measurement condition would act primarily as a common background rather than a shape-specific term. Under these conditions, the extracted $R_{\mathrm{int,vol}}$ represents the interfacial contribution after removal of the independently measured device/buffer resistance. For systems involving different solvents, stronger optical heating, forced flow, or larger temperature gradients, $R_{\mathrm{fluid,vol}}$ should be re-evaluated under the corresponding experimental conditions.

To calculate $h_{\mathrm{conv}}$:

$$R_{\mathrm{fluid,vol}} = \frac{V_{\mathrm{fluid}}}{h_{\mathrm{conv}}\, A_{\mathrm{cell}}} \quad \Longrightarrow \quad h_{\mathrm{conv}} = \frac{V_{\mathrm{fluid}}}{R_{\mathrm{fluid,vol}}\, A_{\mathrm{cell}}}. \tag{S14}$$

From our experimental setup, we know

$$\begin{aligned} V_{\text{fluid}} &= 200\ \mu\text{L} = 2.00 \times 10^{-7}\,\text{m}^3, \\ A_{\text{cell}} &= \pi(5\,\text{mm})^2 = 7.85 \times 10^{-5}\,\text{m}^2, \\ R_{\text{fluid,vol}} &= 1.10 \times 10^{-6}\,\text{m}^3\,\text{K}\,\text{W}^{-1}. \end{aligned} \tag{S15}$$

Therefore,

$$h_{\text{conv}} = \frac{2.00 \times 10^{-7}}{1.10 \times 10^{-6} \times 7.85 \times 10^{-5}} \approx 2.3 \times 10^3\ \text{W}\,\text{m}^{-2}\,\text{K}^{-1}. \tag{S16}$$

We can also evaluate $R_{\text{int,vol}}$ using Eq. S10 with representative values $N_p = 10^{11}$ and $R_{K0} = 5 \times 10^{-9}\,\text{K}\,\text{m}^2\,\text{W}^{-1}$. The geometric factor is

$$g = \frac{D}{L} + \alpha\,\frac{h_{\text{spike}}}{r_{\text{tip}}}. \tag{S17}$$

Example values are:

$$\text{Sphere:} \quad g = \frac{D}{L} = \frac{35\,\text{nm}}{35\,\text{nm}} = 1, \tag{S18}$$

$$\text{Rod:} \quad g = \frac{D}{L} = \frac{10\,\text{nm}}{55\,\text{nm}} \approx 0.182, \tag{S19}$$

$$\begin{aligned} \text{Star:} \quad g &= \frac{D_{\text{core}}}{D_{\text{core}} + 2h_{\text{spike}}} + \alpha\,\frac{h_{\text{spike}}}{r_{\text{tip}}} \\ &= \frac{66\,\text{nm}}{66\,\text{nm} + 2(13.77\,\text{nm})} + 1 \times \frac{13.77\,\text{nm}}{2.0\,\text{nm}} \\ &\approx 0.706 + 6.885 \approx 7.591. \end{aligned} \tag{S20}$$

The nanostar geometry factor is particularly sensitive to $r_{\text{tip}}$ because the curvature contribution enters through $h_{\text{spike}}/r_{\text{tip}}$. Therefore, uncertainty in the spike-tip radius produces a larger and asymmetric uncertainty in the nanostar geometry factor compared with spheres and rods. For calculation of nanoparticle volume and surface area, we use the following expressions:

$$V_{\text{NP}}^{(\text{sphere})} = \frac{4}{3}\pi R^3, \qquad A_{\text{NP}}^{(\text{sphere})} = 4\pi R^2. \tag{S21}$$

$$V_{\text{NP}}^{(\text{rod})} = \pi r^2 L, \qquad A_{\text{NP}}^{(\text{rod})} = 2\pi r L + 2\pi r^2. \tag{S22}$$

$$V^{(\text{cone})} = \frac{1}{3}\pi r^2 h, \qquad A_{\text{lateral}}^{(\text{cone})} = \pi r\sqrt{r^2 + h^2}. \tag{S23}$$

$$V_{\text{NP}}^{(\text{star})} = \frac{4}{3}\pi R^3 + n\left(\frac{1}{3}\pi r^2 h\right), \qquad A_{\text{NP}}^{(\text{star})} = 4\pi R^2 + n\left(\pi r\sqrt{r^2 + h^2} + \pi r^2\right). \tag{S24}$$

Using these values, we compute the total volume-normalised heat-transfer resistance and compare it with experimental data. The experimental time traces are fitted using the reduced dark and illuminated forms derived below from Eqs. S1 and S2.

## 1.1 Dark condition ($P_{\mathrm{abs}} = 0$)

Because the electron–phonon coupling constant $G$ is large, electron–lattice equilibration occurs over the fast timescale

$$\tau_{e\text{-}ph} \sim \frac{C_e}{G}. \tag{S25a}$$

This timescale is much shorter than the experimentally measured thermal relaxation time. Therefore, for the experimental time window $t \gg \tau_{e\text{-}ph}$, the electron and lattice temperatures can be treated as nearly equilibrated:

$$T_e(t) \approx T_\ell(t) \equiv T(t). \tag{S25b}$$

Under this single-temperature limit, adding Eqs. S1 and S2 gives

$$(C_e + C_\ell)\,\frac{dT}{dt} = P_{\mathrm{abs}}(t) - \frac{T - T_b}{R_{\mathrm{th,vol}}}. \tag{S25c}$$

Since the electronic heat capacity of Au is much smaller than the lattice heat capacity under the present conditions, $C_e \ll C_\ell$, the effective heat capacity is approximated as

$$C_e + C_\ell \approx C_\ell. \tag{S25d}$$

For the dark condition, $P_{\mathrm{abs}} = 0$, and the reduced thermal balance becomes

$$C_\ell \frac{dT}{dt} = -\frac{T - T_b}{R_{\mathrm{th,vol}}}. \tag{S26}$$

Dividing both sides by $C_\ell$:

$$\frac{dT}{dt} + \frac{1}{C_\ell R_{\mathrm{th,vol}}} T = \frac{1}{C_\ell R_{\mathrm{th,vol}}} T_b. \tag{S27}$$

Define $\tau \equiv C_\ell R_{\mathrm{th,vol}}$, then

$$\frac{dT}{dt} + \frac{1}{\tau} T = \frac{T_b}{\tau}. \tag{S28}$$

Using the integrating factor $\mu(t) = e^{t/\tau}$:

$$\frac{d}{dt}\left[e^{t/\tau} T\right] = \frac{T_b}{\tau} e^{t/\tau}. \tag{S29}$$

Integrating from 0 to $t$:

$$e^{t/\tau} T(t) - T(0) = T_b\left(e^{t/\tau} - 1\right). \tag{S30}$$

Solving for $T(t)$:

$$T(t) = T_b + \left[T(0) - T_b\right] e^{-t/\tau}. \tag{S31}$$

The volume-normalised measured resistance in the dark is defined as

$$R_m(t) \equiv \frac{T(t) - T_b}{P_0}. \tag{S32}$$

Substituting Eq. (S31) into Eq. (S32) gives

$$R_m(t) = \frac{T(0) - T_b}{P_0} e^{-t/\tau} = R_m(0) e^{-t/\tau}. \tag{S33}$$

## 1.2 Illuminated condition ($P_{\text{abs}} > 0$)

Using the same single-temperature and $C_e \ll C_\ell$ approximation, but now with $P_{\text{abs}} > 0$, the reduced thermal balance becomes

$$C_\ell \frac{dT}{dt} = P_{\text{abs}} - \frac{T - T_b}{R_{\text{th,vol}}}. \tag{S34}$$

Dividing by $C_\ell$:

$$\frac{dT}{dt} + \frac{1}{\tau} T = \frac{P_{\text{abs}}}{C_\ell} + \frac{T_b}{\tau}. \tag{S35}$$

Using the integrating factor $\mu(t) = e^{t/\tau}$:

$$\frac{d}{dt}\left[e^{t/\tau} T\right] = \left(\frac{P_{\text{abs}}}{C_\ell} + \frac{T_b}{\tau}\right) e^{t/\tau}. \tag{S36}$$

Integrating from 0 to $t$:

$$e^{t/\tau} T(t) - T(0) = \left(\frac{P_{\text{abs}}}{C_\ell} + \frac{T_b}{\tau}\right) \left(e^{t/\tau} - 1\right). \tag{S37}$$

Solving for $T(t)$:

$$T(t) = T_b + P_{\text{abs}} R_{\text{th,vol}} + \left[T(0) - T_b - P_{\text{abs}} R_{\text{th,vol}}\right] e^{-t/\tau}. \tag{S38}$$

## 1.3 Measured resistance in light

The volume-normalised measured resistance under illumination is

$$R_m(t) = \frac{T(t) - T_b}{P_0 + P_{\text{abs}}}. \tag{S39}$$

Substituting Eq. (S38) into Eq. (S39) gives

$$R_m(t) = \frac{P_{\text{abs}} R_{\text{th,vol}}}{P_0 + P_{\text{abs}}} + \left[\frac{T(0) - T_b}{P_0 + P_{\text{abs}}} - \frac{P_{\text{abs}} R_{\text{th,vol}}}{P_0 + P_{\text{abs}}}\right] e^{-t/\tau}. \tag{S40}$$

Define

$$R_\infty \equiv \frac{P_{\text{abs}} R_{\text{th,vol}}}{P_0 + P_{\text{abs}}}, \qquad R_0 \equiv R_m(0), \qquad \tau = C_\ell R_{\text{th,vol}}. \tag{S41}$$

Then

$$R_m(t) = R_\infty + (R_0 - R_\infty)\, e^{-t/\tau}. \tag{S42}$$

## 1.4 Summary of equations used for fitting dark and light-on conditions

Time constant:

$$\tau = C_\ell R_{\mathrm{th,vol}}. \tag{S43}$$

Dark decay with nonzero experimental baseline:

$$R_m(t) = R_0 e^{-t/\tau} + C, \qquad C = R_m(\infty). \tag{S44}$$

Light decay:

$$R_m(t) = R_\infty + (R_0 - R_\infty)\, e^{-t/\tau}. \tag{S45}$$

After fitting the dark and illuminated conditions with Eqs. S44 and S45, respectively, the extracted time constant $\tau$ is used to obtain the volume-normalised thermal resistance as $R_{\mathrm{th,vol}} = \tau/C_\ell$. The corresponding absolute thermal resistance is then obtained from $R_{\mathrm{th}} = R_{\mathrm{th,vol}}/V_{\mathrm{fluid}} = \tau/(C_\ell V_{\mathrm{fluid}})$.

## 1.5 Conditions for fitting dark with Eq. S44

When nanoparticle suspension is added onto the 37 °C heater chip, the measurement does not start from zero thermal signal. There is already a steady heat input from the copper block, represented by $P_0$ in the same volumetric convention used above, across the particle–liquid interface that maintains $T_2$ at an offset above room temperature. This baseline persists even after the injection transient has decayed. Therefore, instead of the simpler form $R_0 e^{-t/\tau}$, the dark data are fitted using

$$R_m(t) = R_0 e^{-t/\tau} + C.$$

Here, $C$ explicitly accounts for the nonzero background, $C = R_m(\infty)$. If $C$ were omitted, the fit would be forced to return to zero as $t \to \infty$, misrepresenting the constant heater-driven $\Delta T_\infty$ and biasing both $\tau$ and $R_{\mathrm{th,vol}}$. Including $C$ is therefore necessary to separate the pure exponential decay from the baseline thermal resistance that is always present in the dark measurements.

## 1.6 Thermal resistance device set-up

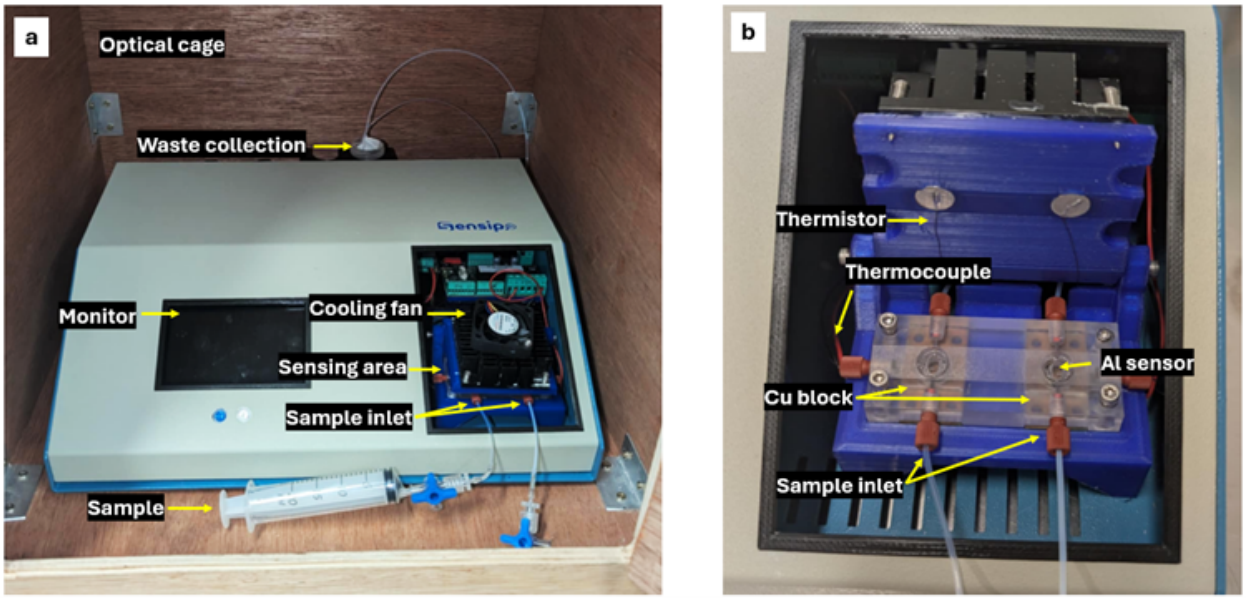


Figure S1: Thermal resistance device setup: **(a)** Thermal resistance device showing the sample inlet, sensing area, and waste collection zone and **(b)** close-up of the sensing module with the cooling fan lifted, revealing the positions of the thermistor, thermocouple, Cu block, and Al sensor.

# References


[1] X. Chen, A. Munjiza, K. Zhang, and D. Wen, "Molecular dynamics simulation of heat transfer from a gold nanoparticle to a water pool," *The Journal of Physical Chemistry C*, **118**, 1285–1293 (2014).

[2] S. Merabia, S. Shenogin, L. Joly, P. Keblinski, and J.-L. Barrat, "Heat transfer from nanoparticles: A corresponding state analysis," *Proceedings of the National Academy of Sciences*, **106**, 15113–15118 (2009).

[3] O. Gutiérrez-Varela, A. Ramos-Alvarado, and S. Kumar, "Size-dependent effects of the thermal transport at gold–water interfaces," *The Journal of Chemical Physics*, **157**, 084702 (2022).

[4] R. Rabani, M. H. Saidi, A. Rajabpour, L. Joly, and S. Merabia, "Enhanced heat flow between charged nanoparticle and aqueous electrolyte," *Langmuir*, **39**, 17701–17711 (2023).